On the Role of Stochastic Channel Behavior in Intracellular Ca^{2+} Dynamics

Martin Falcke
Hahn Meitner Institute, Glienicker Str. 100, 14109 Berlin, Germany and Max Planck Institute for the Physics of Complex Systems, Nöthnitzer Str. 38, 01187 Dresden, Germany

ABSTRACT I present a stochastic model for intracellular Ca^{2+} oscillations. The model starts from stochastic binding and dissociation of Ca^{2+} to binding sites on a single subunit of the IP_3-receptor channel but is capable of simulating large numbers of clusters for many oscillation periods too. I find oscillations with variable periods ranging from 17 s to 120 s and a standard deviation well in the experimentally observed range. Long period oscillations can be perceived as nucleation phenomenon and can be observed for a large variety of single channel dynamics. Their period depends on the geometric characteristics of the cluster array. Short periods are in the range of the time scale of channel dynamics. Both long and short period oscillations occur for parameters with a nonoscillatory deterministic regime.

INTRODUCTION

The beauty of intracellular Ca^{2+} dynamics is that it allows for observation of the build up of periodic global events from local stochastic events. A theoretical analysis on how the stochasticity of the elemental events shows up in the global events is the subject of this article.

Changes in the cytosolic free Ca^{2+} concentration are used by many cells for signaling (Tsien and Tsien, 1990; Berridge et al., 1998). The rise of that concentration is accomplished beside influx through the plasma membrane by release of Ca^{2+} from intracellular stores like the endoplasmic reticulum (ER). Opening and closing of Ca^{2+} channels on the ER membrane controls the release. Channels are closely packed into clusters (Sun et al., 1998; Thomas et al., 1998; Mak et al., 2000; Mak and Foskett, 1998). The clusters are randomly distributed on the ER membrane. Areas with high cluster density are called focal sites (Lechleiter et al., 1991; Callamaras and Parker, 2000; Marchant and Parker, 2001). Channels open and close stochastically. Stochastic behavior manifests itself as spontaneous release events through single channels or several channels in a cluster (Sun et al., 1998; Callamaras and Parker, 2000; Marchant and Parker, 2001; Thomas et al., 1999; Bootman et al., 1997a).

A channel type present in the ER membrane of many cells is the inositol 1,4,5-trisphosphate (IP_3) receptor channel (IP_3R). The open probability of the IP_3R depends on the calcium concentration on the cytosolic side of the channel and the IP_3 concentration (Taylor, 1998; Patel et al., 1999). It increases nonlinearly with the IP_3 concentration and the Ca^{2+} concentration. Hence, Ca^{2+} released by one channel increases the open probability for neighboring channels. That provides a self-amplifying release mechanism. Very high Ca^{2+} concentration inhibits the channel and terminates release.

Another element of intracellular Ca^{2+} handling are buffers. Buffers are proteins binding most of the Ca^{2+} in a cell (up to 99%). They are present in the cytosol as well as the ER. Buffers are considered as mobile or immobile depending on their diffusion characteristics. The rate constants of Ca^{2+} binding and dissociation allow for a distinction between slow and fast buffers.

The dependence of the open probability of the release channels on cytosolic Ca^{2+} creates communication between channels and allows for the formation of spatiotemporal patterns of intracellular Ca^{2+} release. These patterns show a hierarchy of phenomena. The smallest event is the opening of a single channel, called a blip. The next larger event is called puff and is the opening of several closely packed channels. Puffs can cooperate to set off a wave traveling through the cell. Waves would appear as an elevation of the Ca^{2+} concentration engulfing the whole volume in cells smaller than the wave length. If waves occur periodically, they appear as global oscillations. The type of the dominant pattern depends on the IP_3 concentration with puffs at low and waves and oscillations at high values.

Parker et al. investigated the hierarchy of spatiotemporal events in detail in *Xenopus* oocytes and Bootman et al. in HeLa cells (Marchant et al., 1999; Callamaras et al., 1998; Sun et al., 1998; Marchant and Parker, 2001; Thomas et al., 1999; Bootman et al., 1997a; Bootman et al., 1997b). Typically, a single puff is not enough to initiate a wave (Marchant et al., 1999). Rather, the cooperative action of several puff sites is required. The mechanism by which waves are initiated after a step increase of IP_3 is not an increase in puff amplitude. The amplitude of puffs preceding wave initiation immediately was constant. The way the critical amount of Ca^{2+} is raised is an increasing puff frequency by up to a factor of 10 (Marchant et al., 1999). That causes an elevated average Ca^{2+} concentration at the site of wave initiation before the start of the wave (Marchant et al., 1999).

Submitted June 25, 2002, and accepted for publication August 30, 2002.
Address reprint requests to M. Falcke, Hahn Meitner Institute, Glienicker Str. 100, 14109 Berlin, Germany. Tel.: 49-30-80622627; Fax: +49-30-80622098; E-mail: falcke@hmi.de.

0006-3495/03/01/42/15 $2.00

The necessity for cooperativity of several puffs to initiate a wave allows for the occurrence of single puffs in between consecutive waves. Marchant et al. measured the characteristics of these puffs dependent on wave phase and period (Marchant and Parker, 2001). The measurements demonstrate typical differences between repetitive wave initiation with short and long periods. The peak of the previous wave was chosen as the reference time in the presentation of the results of the experiments (Marchant and Parker, 2001). Puffs did not occur in the first 7 s after a wave passed. Then, puffs occurred with increasing frequency. That increase continued until initiation of the next wave for short period waves ($<$15 s). The puff amplitude quickly reached a certain level which then stayed constant for the last 30–40% of the wave period. Waves with intermediate periods (15–50 s) exhibit an increase in puff frequency from 7 s after the previous wave until about three quarters through the cycle. The amplitude again soon reaches its steady level which it then keeps for most ($\approx$60%) of the cycle. Finally, waves with periods longer than 50 s did not show any essential variation in puff amplitude or puff frequency during the 60% of the wave cycle preceding the next wave (Marchant and Parker, 2001).

A noticeable difference between short and long period waves is revealed by looking at base level Ca^{2+} concentration at the site of wave initiation (Marchant and Parker, 2001). It declines until emergence of the next wave between short period waves. Base level Ca^{2+} reaches a minimum at about half the period and then slowly rises until initiation of the next wave between long period waves. That increase in base level Ca^{2+} preceding waves was called pacemaker Ca^{2+}.

A wide range of periods was found in *Xenopus* oocytes with the shortest ones of $\approx$10 s and the longest ones up to 2 min (Marchant and Parker, 2001). The time necessary for inhibition of the channels and recovery from it is $\sim$10 s in *Xenopus* oocyte (Ilyin and Parker, 1994) and is in the range of the short periods. Hence, the dynamics of the channel alone cannot account for the long period oscillations of 60 s and more.

Especially for long period waves, the nucleation of a wave by the cooperative action of a few puffs could be demonstrated (Marchant et al., 1999). Activity of a single puff site is typically not sufficient to set off a wave but it needs a supercritical nucleus formed by a few puff sites for the wave to be initiated. Because puffs are stochastic events, the formation of such a supercritical nucleus occurs with a certain probability only. Marchant and Parker (2001) state that the time elapsing between two consecutive waves is determined by two processes: The recovery from inhibition caused by the first wave and the creation of a supercritical nucleus for the second wave (Marchant and Parker, 2001). The probabilistic character of nucleation introduces variability into the wave period. Marchant et al. report a standard deviation up to 40% for long period waves (Marchant and Parker, 2001). That supports the interpretation of long period repetitive waves as nucleation phenomena.

I address the stochastic modeling of nucleation and the complete range of oscillation periods. The purpose of that effort is to check Parker's hypothesis on repetitive wave nucleation during long period oscillations from a theoretical point of view. There are interesting questions linked to that. What determines the nucleation probability? Given the fact that the periods are much longer than any process of the channel dynamics (Sneyd et al., 1995), what is the role of single channel dynamics then? The small number of channels involved into formation of a single puff makes it obvious that puffs should be random events. This is less obvious for nucleation processes involving several clusters—i.e., a few times more channels—because fluctuations decrease like $\sqrt{n}^{-1}$ with n being the number of elements involved. Will wave nucleation show stochastic behavior or resemble more a deterministic process? If it is stochastic with a nucleation probability small enough to account for long periods, would the standard deviation of the period be in the right range? Last but not least, the intracellular Ca^{2+} dynamics offers a unique opportunity to investigate the build up of global events from stochastic elemental events.

Starting point of a model for our purposes has to be of course the behavior of a single channel and its subunits as the major source of stochasticity. At the same time the model needs to be extended to length scales of several cluster spacings and simulations lasting several long periods have to be carried out. In technical terms, I intend to model a wide range of time scales (from activation of the subunit by Ca^{2+} in the milliseconds range to several periods i.e., $\approx$1000 s) and length scales (single cluster $\approx$100 nm to several cluster spacings $\approx$100 μm). Recently, we introduced a simulation concept for intracellular Ca^{2+} handling especially suited for that task. It takes into account the spatially discrete arrangement of channel clusters as well as the stochastic behavior of single channel subunits (Falcke et al., 2000b). Single subunit dynamics was represented as a stochastic realization of the DeYoung-Keizer model. I use that simulation concept as a starting point for the work presented here. The previous simulations included buffering as a constant ratio of free to buffered Ca^{2+}. Here, I extend the simulations by dropping that approximation and consider state dependent buffer ratios.

I will introduce the modeling concept in the next section. The simulations show oscillation-like behavior with an average period and its standard deviation covering the complete range observed in experiments. Long period oscillations are wave nucleation processes depending most strongly on spatial characteristics of the cluster array and the number of channels per cluster. Short periods arise because fluctuations prevent the dynamics from settling in a stable stationary focus. Finally, I will show for four different cases with low

and high $[IP_3]$ that the deterministic limit of the stochastic simulation is nonoscillatory.

MATERIALS AND METHODS

The reaction diffusion equations

I describe the interior of the cell as a spatially two-dimensional area with a regular cluster grid with spacing d as the basic arrangement. Focal sites are mimicked by further randomly distributed clusters in certain regions of the area. The number of channels in an individual cluster N_K^i was chosen with a uniform distribution between $N_K^{max}/2$ and N_K^{max} with N_K^{max} being the maximum number of channels per cluster.

The dynamics of the concentrations is determined by release from the endoplasmic reticulum, diffusion, buffering, and uptake of Ca^{2+} by the ER. That can be described by partial differential equations (PDEs):

$$\begin{aligned}
\frac{\partial c}{\partial t} &= D\nabla^2 c + (P_l + P_c(r))(E-c) - P_p\frac{c^2}{K_d^2+c^2} \\
&\quad - H_i(c, b_i) \\
\frac{\partial E}{\partial t} &= D_E\nabla^2 E - \gamma\left[(P_l + P_c(r))(E-c) - P_p\frac{c^2}{K_d^2+c^2}\right] \\
&\quad - H_j(c, b_{E,j}) \\
\frac{\partial b_i}{\partial t} &= H_i(c, b_i) = D_{b,i}\nabla^2 b_i + k_{b,i}^+(B_i - b_i)c - k_{b,i}^- b_i, \\
&\quad i = s, ex, m \\
\frac{\partial b_{E,j}}{\partial t} &= H_j(E, b_{E,j}) = D_{E,j}\nabla^2 b_{E,j} + k_{E,j}^+(G_i - b_{E,j})E - k_{E,j}^- b_{E,j}, \\
&\quad j = s, m.
\end{aligned} \tag{1}$$

The channel clusters enter the PDE for the cytosolic Ca^{2+} concentration c through the factor of the Ca^{2+} source term P_c. It depends on the spatial coordinate r: $P_c = P_c(r)$. $P_c(r)$ vanishes outside a cluster and assumes the spatially constant positive value P inside. The number of open channels inside a cluster is represented by the size of the area where $P_c(r) = P$. The radius R_c of that area is determined as $R_c = \sqrt{N_O}R_s$, where R_s is the single channel radius and N_O the number of open channels in the cluster. The single channel radius is 35 nm in most of the simulations. That is not meant to be the radius of the pore of an ion channel. Rather, it is supposed to be the size of the area where the Ca^{2+} concentration is essentially spatially homogeneous. Swillens et al. (1998) showed that it is not necessary to resolve smaller length scales for the concentration gradients occurring around a channel. Hence, the exact geometry of the Ca^{2+} source within that volume can be neglected. Furthermore, that choice of R_s describes a channel by at least three points of the numerical grid in radial direction, improving numerical accuracy. The variable E is the free Ca^{2+} concentration in the ER.

Buffers with Ca^{2+} bound in the cytosol are denoted b_i, those in the ER $b_{E,j}$. I do not consider any slow buffers for the time being but will deal with them in a later paper (Falcke, 2003). Immobile buffers are modeled by setting their diffusion coefficient equal to 0. Cytosolic buffers comprise endogenous stationary buffer b_s, endogenous mobile buffer b_m and exogenous mobile buffer b_{ex}. The buffers in the ER are an endogenous immobile buffer b_{Es} and an endogenous mobile buffer b_{Em}.

The components of the vector $\mathbf{N_O}(t)$ are the numbers of open channels of all clusters. That vector is obtained from the stochastic simulation for the channel dynamics coupled to the solution of Eq. 1 (see below). I assume that the dynamics of the different concentrations are sufficiently fast so that the concentration fields reach the stationary solution before $\mathbf{N_O}(t)$ changes. That allows for taking the stationary solution of Eq. 1 belonging to the current $\mathbf{N_O}(t)$ as the profile of the concentration field until $\mathbf{N_O}(t)$ changes. That approximation based on differential time scales is called adiabatic approximation. The details of how this is done are explained in the last section of this article.

The adiabatic approximation neglects the time it takes to build up the concentration profiles upon opening of a channel. That is well justified for the concentration at the location of the opening channel itself. The approximation neglects the 100–200 ms it takes for Ca^{2+} to diffuse to the neighboring cluster. One consequence is that wave speeds would be overestimated with that approach. Therefore, I do not consider them here. I will suggest a way of mapping the results of our simulations onto results of simulations with fully time dependent diffusion in the discussion section. Similarly, the slow decrease of pacemaker Ca^{2+} after closing of a channel is neglected. I will discuss that as well below.

The stochastic channel dynamics

I adopt the DeYoung-Keizer model for the subunit dynamics (DeYoung and Keizer, 1992; Keizer and DeYoung, 1994). An IP_3R consists of four identical subunits in the framework of that model. There are three binding sites on each subunit: An activating site for Ca^{2+}, an inhibiting Ca^{2+} site and an IP_3 binding site. The three binding sites allow for eight different states X_{ijk} of each subunit. The index i stands for the IP_3 site, j for the activating Ca^{2+} site, and k for the inhibiting Ca^{2+} site. An index is 1 if an ion is bound and 0 if not. Transition probabilities per unit time of transitions involving binding of a molecule are proportional to the concentration of that molecule. Dissociation transition probabilities per unit time are constant. I assume that the channel is open if at least three of the subunits are in X_{110}, i.e., they have bound Ca^{2+} at the activating site and IP_3.

The experimental analog to the state "open" is actually a rapid switching between an open and a closed state of the channel with much higher open probability than other states (see e.g., (Moraru et al., 1999; Mak et al., 2001)). However, the consequence for the slow dynamics is the same as that of a current averaged in time over the rapid opening and closing because the transition probabilities depend on the time integral of the Ca^{2+} concentration ($\int dtc(t)$) only. On that basis, I use a constant current through the channel when the channel is in the open state.

According to (DeYoung and Keizer, 1992), the transition rates between the states X_{0jk} and X_{1jk} (IP_3 binding and dissociation) are two orders of magnitude faster than the other transition rates (see Table 1). Therefore, these pairs of states will reach stationary probabilities before the states of the Ca^{2+} binding sites change. Hence, we can lump the pairs X_{0jk} and X_{1jk} into single states $X_{jk} = X_{0jk} + X_{1jk}$.

The binding probability of IP_3 is included into the model by using only the average fraction of the N_K^i channels of a cluster which can be activated by Ca^{2+} binding to the activating sites alone, i.e., that fraction which has IP_3 bound to at least three subunits. I denote the probability that IP_3 is bound when Ca^{2+} is bound to the activating site at one subunit p_I ($p_I = I/(d_1 + I)$). The probability p_I^c that IP_3 is bound to at least three out of the four subunits is given by $p_I^c = 4p_I^3 - 3p_I^4$. That fraction $p_I^c N_K^i$ of N_K^i is the IP_3-dependent number of channels of the ith cluster used in the simulation.

The kinetic scheme with the lumped states is shown in Fig. 1. The state with no Ca^{2+} ion bound is X_{00}, the activated state is X_{10} and the inhibited states are X_{11} and X_{01}. The binding and dissociation of Ca^{2+} at the activating and inhibiting sites are stochastic events rendering the opening and closing of the channel a stochastic process. That stochastic process is coupled to the concentration of cytosolic Ca^{2+} because the binding probabilities per unit time depend on it and vice versa the number of open channels determines the concentration field.

Single cluster profiles

We have a complete description of intracellular Ca^{2+} release with the Eq. 1 and the stochastic scheme in Fig. 1 by now and can start to simulate. I show

TABLE 1 Parameters for stochastic simulations

Parameter	Value	Unit
Leak flux coefficient P_l	0.0025	s^{-1}
Channel flux coefficient P	600	s^{-1}
Single channel radius R_s	0.0354	μm
Cluster spacing outside focal sites	4.33	μm
Max. number of channels per cluster N_K^{max}	25	
Number of additional clusters in focal sites N_F	5	
Pump flux coefficient P_p	40	$\mu M\ s^{-1}$
Pump dissociation coefficient K_d	0.2	μM
Volume ratio V_{cyt}/V_{ER}	10.0	
Diffusion coefficient D of free cytosolic Ca^{2+}	223	$\mu m^2\ s^{-1}$
Diffusion coefficient D_E of free lumenal Ca^{2+}	40	$\mu m^2\ s^{-1}$
Diffusion coefficient D_m of cytosolic endogenous mobile buffer	11.26	$\mu m^2\ s^{-1}$
Diffusion coefficient D_{ex} of cytosolic exogenous buffer	32.0	$\mu m^2\ s^{-1}$
Diffusion coefficient D_{Em} for lumenal mobile buffer	1	$\mu m^2\ s^{-1}$
On-rates of fast buffers: $k_s^+, k_m^+, k_{ex}^+, k_{Es}^+, k_{Em}^+$	500	$(\mu M\ s)^{-1}$
Dissociation constants of buffers k_i^-/k_i^+ :		
K_s	2	μM
K_m	2	μM
K_{ex}	0.247	μM
K_{Es}	500	μM
K_{Em}	5	μM
Total concentrations of buffers:		
B_s	200	μM
B_m	50	μM
B_{ex}	60	μM
B_{Es}	100	mM
B_{Em}	5	mM
Total concentration of Ca^{2+} C_0	5.385	mM
Subunit kinetics, note $b_i = a_i d_i, i = 1, \ldots, 5$		
a_2, a_4	0.0555	$(\mu M\ s)^{-1}$
a_5	2.222	$(\mu M\ s)^{-1}$
d_1	0.13	μM
d_2	3.776	μM
d_3	0.9434	μM
d_4	0.5202	μM
d_5	0.72	μM
IP_3 concentration I	0.15	μM
a_6 (see Fig. 1)	$\frac{a_2 I + a_4 d_1}{d_1 + I}$	
b_6 (see Fig. 1)	$\frac{b_2 I + b_4 d_3}{d_3 + I}$	

a snapshot taken from a simulation in Fig. 2. It is the concentration of fast high affinity buffer (b_{ex}). The total number of open channels for two simulations is shown in Fig. 3. The simulation was carried out with high fast buffer concentration. Single channel openings do not lead to higher activity for a long time but then the system switches to a state with a maintained activity of $\approx$10 open channels. The simulations shown in Figs. 2 and 3 were done by solving Eqs. 8 and 9 for each $\mathbf{N_O}(t)$. That is computationally expensive. A single run of 100 s real time takes several hundred hours of cpu time. That is one of the motivations to approximate the complete solution of concentration fields by the superposition of single cluster profiles. Besides that, the single cluster profiles are a convenient picture to understand what happens during the simulations.

The Ca^{2+} concentration around a single cluster with open channels is strongly localized as can be seen in the plot of a single cluster concentration profile shown in Fig. 4 *A*. The high Ca^{2+} concentration at the open channels decreases by a factor of 0.0303 on the distance of cluster spacing in the

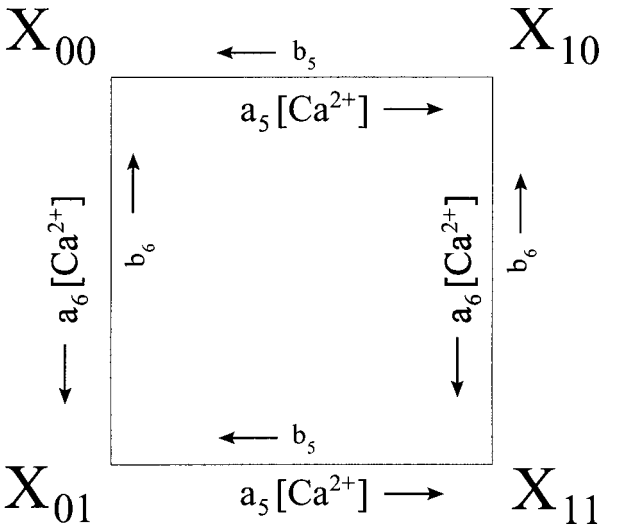

FIGURE 1 Lumped states X_{jk} of a subunit of the IP_3 receptor channel. An index is 1 if an ion is bound and 0 if not. The index j stands for the activating Ca^{2+} site and k for the inhibiting Ca^{2+} site. The transition rates are given at the edges of the rectangle.

example of Fig. 4 *A*. That decrease can be considered as a measure of localization. I take advantage of localization to simplify the solution of Eq. 1 for a large array of clusters by representing the full solution as a superposition of single cluster profiles.

I introduce the concentration vector $\mathbf{U}(r, A^0, \mathbf{N_O}(t))$ consisting of the elements $\{c^0, E^0, b_s^0, b_{ex}^0, b_m^0, b_{Es}^0, b_{Em}^0\}$. The single cluster profile $\mathbf{U}^s(r - r_i, A^0, N_O^i)$ is defined as the stationary solution of Eq. 8 for a single cluster at the position r_i in the center of a large area with no flux boundary conditions and N_O^i open channels. The dependence on the number of open channels is included by choosing the size of the cluster area proportional to N_O^i. The base level of concentrations $\mathbf{U}_b$ is the solution with all channels closed. $\mathbf{U}_b$ is calculated as the solution of Eq. 8 with all channels closed and

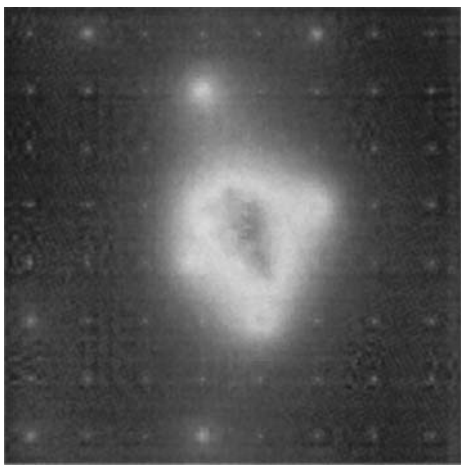

FIGURE 2 Concentration of fast buffer with high affinity as solution of the fully coupled Eqs. 8 and 9. $B_{ex} = 800\ \mu$M, $IP_3 = 0.66\ \mu$M, $B_s = 200\ \mu$M, $B_m = 0$, $B_{Es} = 200\ \mu$M, $K_{Es} = 5\ \mu$M, $B_{Em} = 0$, $C_o = 72\ \mu$M, $[IP_3] = 0.24\ \mu$M, $P = 800\,s^{-1}$, $P_l = 0.001\ s^{-1}$, $P_p = 50\ \mu M\ s^{-1}$, $d = 3.84\ \mu$m, $R_s = 84$ nm. The integration area is $30.72 \times 30.72\ \mu m^2$ and contains 8×8 clusters and a focal site with $N_F = 10$ on a $1.6d \times 1.6d$ area.

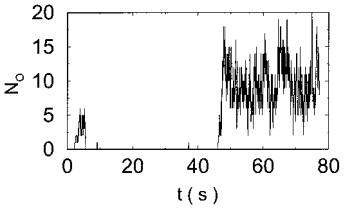

FIGURE 3 Global number of open channels N_o in a simulation solving the fully coupled Eq. 8 and 9 for the concentrations. $[IP_3]$ was kept at 0.06 μM until $t = 10$ s and then set to 0.24 μM. $B_{ex} = 450$ μM, $B_{slow} = 20$ μM, $B_s = 200$ μM, $B_m = 0$, $B_{Es} = 200$ μM, $K_{Es} = 5$ μM, $B_{Em} = 0$, $C_o = 72$ μM, $P_c = 800\,s^{-1}$, $P_c = 0.001\,s^{-1}$, $P_p = 50$ μM s^{-1}, $d = 3.84$ μm, $Rs = 84$ nm. The integration area is 30.72×30.72 μm^2 and contains 8×8 clusters.

with the current A^0. We can superpose only concentration profiles decaying to zero for large distances from the cluster. That is the case with the contribution of open channels to the concentrations i.e., $\mathbf{U}^s(r - r_i, A^0, N_O^i) - \mathbf{U}_b$. The complete concentration field is then formed as the base level plus the sum of all contributions from open channels:

$$\mathbf{U}(r, A^0, \mathbf{N_O}) = \mathbf{U}_b + \sum_i [\mathbf{U}^s(r - r_i, A^0, N_O^i) - \mathbf{U}_b]. \qquad (2)$$

A single cluster profile of free cytosolic Ca^{2+} is plotted in Fig. 4 *A*. The concentration of free Ca^{2+} enters the channel dynamics as a factor of the transition probabilities for transitions representing Ca^{2+}-binding events. Hence, rather than the absolute values of free Ca^{2+}, the change in these transition probabilities per time unit relative to those at the base level concentration c_b is relevant. They are shown in Fig. 4, *B–D* dependent on the number of open channels in a cluster.

Puffs do not show any essential variation in amplitude when IP_3 is increased (Marchant and Parker, 2001; Sun et al., 1998). That might be due

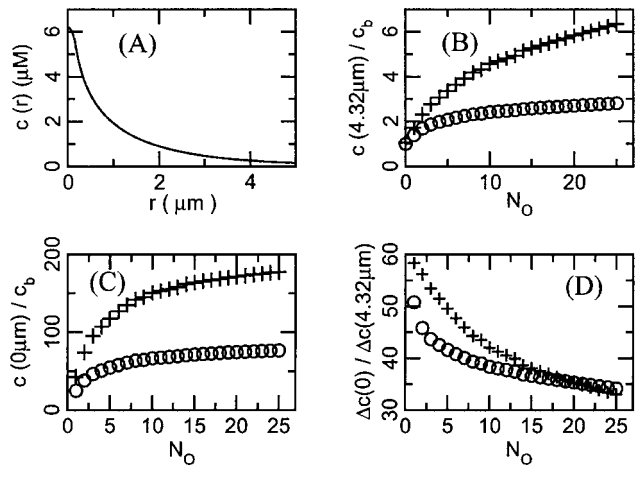

FIGURE 4 Characteristics of single cluster profiles of free Ca^{2+}. (*A*) Free Ca^{2+} dependent on the distance from the cluster center for a cluster with 10 open channels. (*B*) Concentration increase of free Ca^{2+} relative to the base level c_b at a distance of 4.32 μm, used in some simulations as cluster spacing d, dependent on the number of open channels in a cluster. (*C*) Concentration increase of free Ca^{2+} relative to the base level c_b at the center of the cluster. (*D*) Ratio of the contribution of the open channels $\Delta c = c - c_b$ (c_b base level) at $r = 0$ to the contribution at $r = d = 4.32$ μm. Circles refer to calculations with $B_{ex} = 40$ μM and crosses to $B_{ex} = 0$.

to saturation of the free Ca^{2+} peak value with increasing numbers of open channels. Such a saturation can be caused by slow diffusion in the ER. It was shown that diffusion in the ER hindered by a tubular shape can be taken into account by reducing the diffusion coefficient by about a factor of 1/2 compared to unobstructed space (ölveczky and Verkman, 1998). A further reduction of intraluminal diffusion may be due to a higher viscosity compared to the cytosol. However, high viscosity in the ER is an assumption only because I do not know any experimental indication for that. To obtain saturation of peak Ca^{2+} with an increasing number of open channels I reduced diffusion by a factor of 1/5.5 altogether (see Fig. 4, *B* and *C*). The constant puff amplitude observed in experiments may have other causes (e.g., buffer saturation). However, I have chosen to guarantee it by saturating free Ca^{2+}. I show in Falcke (2003) that important results do not depend on that saturation.

Stochastic simulations comprising up to 712 clusters were performed on a cluster array like shown in Fig. 5. Clusters were arranged on a hexagonal grid with a few additional clusters scattered in between to mimic focal sites (see Fig. 5 for details).

Before I present the results of the simulations, I would like to summarize the procedure of one iteration step. Starting from a given configuration of open clusters $\mathbf{N_O}(t)$, I calculate the complete concentration field by superposition of the single cluster profiles ensuring conservation of the total Ca^{2+}. That concentration field determines the probabilities for the random transition to the next state of $\mathbf{N_O}(t)$. That state is obtained by one step of a stochastic simulation for each channel subunit.

RESULTS

A set of simulations for different IP_3 concentrations is shown in Fig. 6. Only puffs are found at low concentrations, i.e., release events are localized and not coordinated on a length scale of several cluster spacings. That changes with the onset of global events at a little bit higher $[IP_3]$ (Fig. 6 *A*). These global events are waves emerging from a nucleation area. They are very rare for low IP_3 concentrations and may travel across the whole system (Fig. 6 *A*, *first* and *second peak*) or fade away before they reach the system boundary (*third peak*). That parameter regime of abortive wave propagation is characterized by a distribution of the probability for a wave

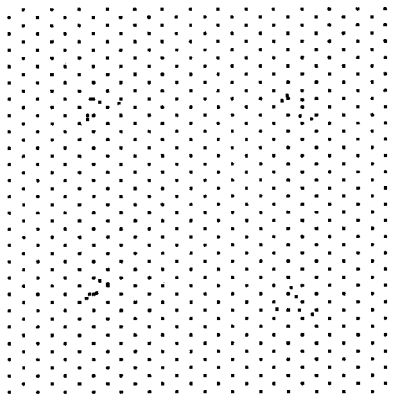

FIGURE 5 Array of clusters used in simulations. The area is quadratic with edge length $L = 120\mu$m. Clusters form a hexagonal grid with distance d. N_F additional clusters are scattered randomly around the points (L/4, L/4), (L/4, 3L/4), (3L/4, L/4), (3L/4, 3L/4) within a square with edge length 2.42 d mimicking a focal site; here $N_F = 5$.

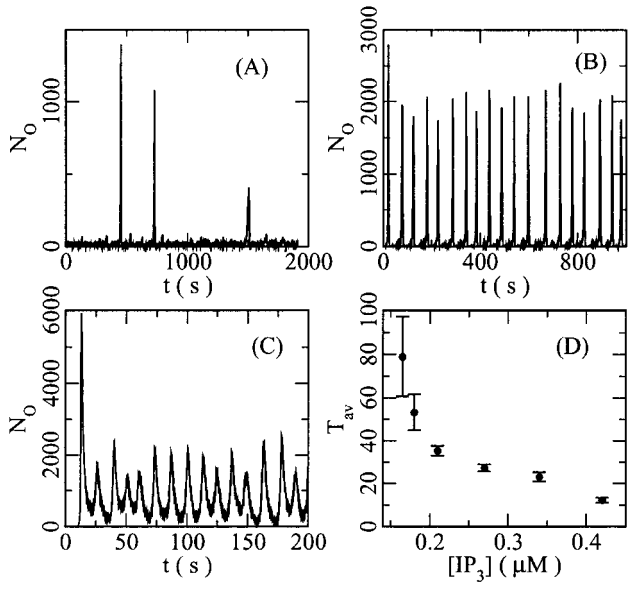

FIGURE 6 Simulations and oscillation characteristics for different IP_3 concentrations: (*A*) $I = 0.15\ \mu M$, (*B*) $I = 0.18\ \mu M$, (*C*) $I = 0.42\ \mu M$, (*D*) T_{av} and its standard deviation dependent on $[IP_3]$.

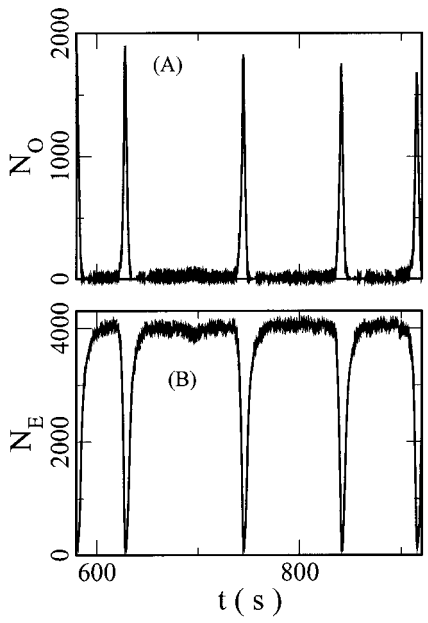

FIGURE 7 The number of open channels (*A*) and the number of excitable channels (at least three subunits in X_{00}) (*B*) during repetitive nucleation of waves. (*A*) is a blow up of panel *B* in Fig. 10. The transition from $X_{01} \rightarrow X_{00}$ was sped up by a factor of 2.5 compared to the standard parameters of Table 1. See Table 1 for parameters except $B_{ex} = 70\ \mu M$ and $N_F = 10$.

to travel a certain distance before being destroyed by fluctuations rather than steadily propagating waves (Falcke et al., 2000b).

Increasing $[IP_3]$ leads to more frequent waves (Fig. 6 *B*) and almost every wave travels across the whole system now. The number of waves within an experimentally relevant time of 2000 s is sufficiently large to determine an average interwave time interval T_{av} and its standard deviation ΔT_{av}, e.g., the simulation shown in (Fig. 6 *B*) has $T_{av} = 53.22 \pm 8.37$ s. Both T_{av} and ΔT_{av} decrease with increasing $[IP_3]$ (Fig. 6 *D*) leading to almost regular oscillations with a period of $\approx$17 s at high $[IP_3]$ (Fig. 6 *C*).

That scenario found while going from low to high $[IP_3]$ agrees with experimental observations (Marchant and Parker, 2001). Especially, the large range of periods of eight times the shortest one reported from the experiments is captured. Short periods could be explained by the longest time scale of the channel dynamics T_d being the transition to the inhibited state and recovery from it. However, long periods last 3–8 times longer and cannot be explained by the channel dynamics alone. That is illustrated in Fig. 7. It shows the number of open channels N_O in panel A and the number of excitable channels N_E in panel B. An excitable channel has at least three subunits in X_{00}. Waves traveling through the whole system appear as spikes in N_O or downward spikes in N_E. N_E reaches again a high level after a wave has passed within $T_d = 18$s. That is far before nucleation of the next wave for at least two of the global events. I have sped up recovery from inhibition ($X_{01} \rightarrow X_{00}$) by a factor of 2.5 in the example shown in Fig. 7 to make this difference between T_d and T_{av} very obvious. That difference demonstrates that the channel dynamics alone cannot account for the long average periods, because the channels are in a state ready to support another wave after time T_d.

To explain the long periods, I start from the observation that waves emerge from small areas—a nucleus—and then spread through the whole system. That is called wave nucleation and is observed in systems like e.g., the FitzHugh-Nagumo model with additive noise (Hempel et al., 1999) or an integrate and fire model with additive noise (Jung and Galley, 2000) as well. Nucleation of global events is probabilistic, because a single puff activates a neighboring cluster with a certain probability only, not with certainty. The nucleation probability p_n is small compared to the puff probability because a supercritical nucleus of a few clusters is needed. The larger a nucleus, the smaller is the curvature of its boundary. The smaller the curvature of the boundary, the larger is the number of active neighbors of an inactive cluster just outside the nucleus and hence the probability for that cluster being activated. That means the larger the nucleus, the larger is the probability that it grows. Deactivation, inhibition, and fluctuations hinder the growth of a nucleus. In that way, a critical size of a nucleus arises.

The nucleation probability is very small just after a wave has traveled across the system because of inhibition of most of the channels by the high Ca^{2+} concentration during the wave. That causes the deterministic part T_d of the time elapsing between two consecutive waves. T_d is determined

essentially by the transition rates from the activated state (X_{10}) to the inhibited state (X_{11}) and recovery from inhibition ($X_{11} \rightarrow X_{01} \rightarrow X_{00}$). However, p_n is still small after recovery from inhibition. Hence, the next wave does not emerge immediately but it takes some time before another global event can be set off. I would like to illustrate that with the example of Fig. 10 *B*. The average period T_{av} of the complete run over 1000 s is ≈65 s. The nucleation probability is the inverse of the stochastic part T_{st} of T_{av}, i.e., $p_n = T_{st}^{-1} = (T_{av} - T_d)^{-1} = 0.021\ s^{-1}$. Hence, the small value of p_n provides for the larger part of T_{av}.

A nucleation is shown in Fig. 8. The puff activity leading to the supercritical event starts in the area marked in Fig. 8 in the frame $t = 370.9$ s. That area is outside but close to a focal site. The area comprises a few clusters and the interaction of these clusters allows for stochastic release to go on for a few seconds. The focal site is activated by the ongoing puff activity in its vicinity (Fig. 8, frame $t = 375.8$ s). It strongly amplifies puff activity and sets off a wave. That wave propagates across the whole simulation area (Fig. 8, frames $t = 380.2$ s, $t = 383.2$ s, $t = 384.3$ s). The maximum number of open channels in panel A occurs when the wave travels through the area marked in frame $t = 370.9$ s. Ca^{2+} release terminates first in the area where the wave started (frame $t = 383.2$ s) due to inhibition. Puff activity is reduced to almost none after the wave ceased (Fig. 8, frame $t = 388.6$ s).

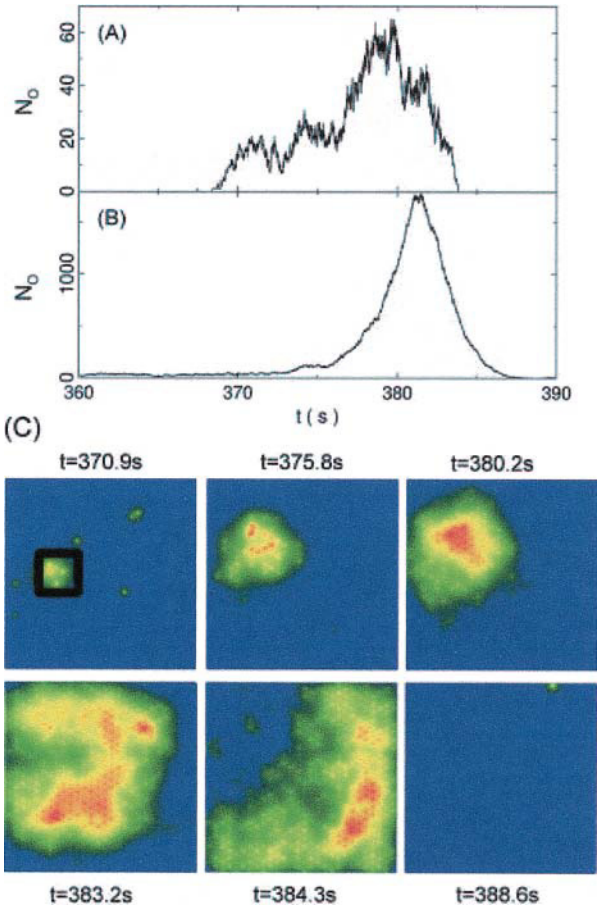

FIGURE 8 Nucleation of a wave in a regime with long wave periods. (*A*) shows the number of open channels in the area where the wave nucleates. The nucleation area is bound by a black rectangle in panel (*C*) frame $t = 370.9$ s and comprises several clusters. (*B*) shows the global number of open channels. (*C*) shows six snapshots of the simulation area taken at the times indicated. Shown is Ca^{2+} bound to exogenous buffer. The color scaling is a minimum–maximum scaling with blue indicating minimal values and red maximal ones.

An example of a release event comprising several clusters which failed to set off a wave—a subcritical nucleus—is shown in Fig. 9. Panel *A* shows the number of excitable channels N_E to demonstrate that the system has recovered from inhibition. Several puffs occur at the same time around $t = 790$ s (*panel B*). However, they do not nucleate a wave and release activity fades away. The number of open channels in an area including additionally the eight neighboring regions shows that activity has not spread or moved. N_O would reach values between 250 and 450 in panel C in case of spreading as can be estimated from panel A of Fig. 8. That failed nucleation together with the nucleation shown in Fig. 8 illustrates that it takes a supercritical number of active clusters to initiate a global event.

If nucleation probability is setting the stochastic part of the period, that part of the period should depend on the system size and number of focal sites. I performed simulations with a system only a quarter in size of that shown in Fig. 5 containing one focal site instead of four in the large systems. The parameters were those of Table 1 except $N_F = 8$. The

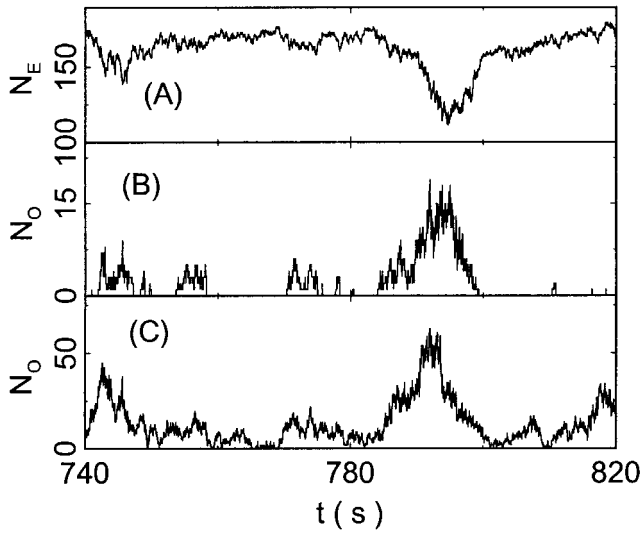

FIGURE 9 The number of excitable channels N_E (at least three subunits in X_{00}) (*A*). The number of open channels in an area of the same size like that marked in panel C of Fig. 8 (*B*). The number of open channels in the same area as in *B* plus the eight neighboring areas of same size (*C*). See Table 1 for parameters except $B_{ex} = 60\ \mu M$ and $I = 0.18\ \mu M$, $d = 5.18\ \mu m$.

average period was 575 s with a deterministic part T_d of ~40 s. The large system has a T_{av} of 177 s with the same T_d. Hence, I obtain a ratio of the stochastic parts of the periods approximately equal to the inverse ratio of system sizes. Jung et al. suggest for a stochastic integrate and fire model that there is an optimal system size with minimal relative standard deviation.

If the nucleation of a wave is the cooperative action of a few clusters, then the nucleation probability p_n should depend very sensitively on parameters determining spatial coupling. Three of these parameters are the buffer concentrations, the cluster spacing and the number of additional clusters in focal sites. Fig. 10 compares simulations with three different concentrations of exogenous mobile buffer B_{ex}. An increase of B_{ex} by 25% extends the average period from 47 ± 10 s to 121 ± 57 s. Varying the cluster spacing leads to a range of periods again from 17 s up to 192 ± 97 s (Fig. 11). Abortive waves occur for large cluster spacing. Waves disappear completely, if the spacing is increased even more. These data show that the average period in the nucleation regime does strongly depend on the strength of spatial coupling.

Because the period depends on spatial coupling, it will as well depend on the number of additional clusters in focal sites or vary for different random realizations with identical average spatial characteristics. That is illustrated in Fig. 12

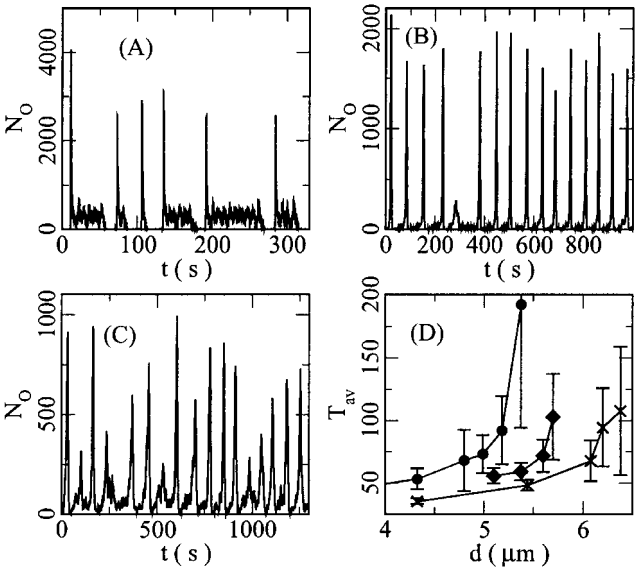

FIGURE 11 Repetitive wave nucleation for different cluster spacing (*A*) $d = 1.594\,\mu$M, $I = 0.18\ \mu$M, (*B*) $d = 4.800\,\mu$m, $I = 0.18\,\mu$M, (*C*) $d = 6.377\ \mu$m, $I = 0.21\,\mu$M. The number of open channels N_O is shown. The small peaks in panel (*C*) are abortive waves. I included an abortive wave into the statistics as a global event, if it traveled across an area larger than 65 μm in diameter. That is the size of the area of observation used by Marchant and Parker (2001). (*D*) shows the period T_{av} and its standard deviation dependent on the cluster spacing. See Table 1 for further parameters except $N_F = 10$, $I = 0.18\,\mu$M (*circles*), $N_F = 5$, $I = 0.195\,\mu$M (*diamonds*), and $N_F = 5$, $I = 0.21\,\mu$M (*x*).

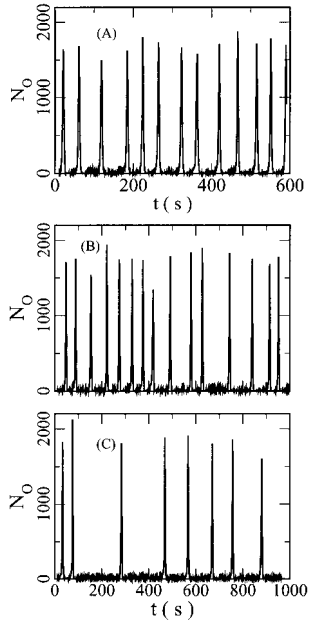

FIGURE 10 Repetitive wave nucleation for three concentrations of exogenous buffer: (*A*) $B_{ex} = 60\ \mu$M, (*B*) $B_{ex} = 70\ \mu$M, (*C*) $B_{ex} = 75\ \mu$M. The number of open channels is shown. The average period is in (*A*) $T_{av} = 47.40 \pm 10.00$ s, (*B*) $T_{av} = 64.55 \pm 23.45$ s and in (*C*) $T_{av} = 121.17 \pm 57.23$ s. The transition from $X_{01} \rightarrow X_{00}$ was sped up by a factor of 2.5 compared to the standard parameters of Table 1. See Table 1 for further parameters except $N_F = 10$.

and Fig. 13. The results for different random realizations of a cluster array (Fig. 13) imply that there are optimal arrays having minimal $\Delta T_{av}/T_{av}$. The array of Fig. 13 *B* has the smallest $\Delta T_{av}/T_{av}$ of 0.214 out of the three examples shown.

I have shown long period oscillations for different parameters of the channel dynamics up to now (e.g., Figs. 10 and 11). That suggests that long period oscillations are possible for a variety of parameters of the local dynamics. I show that again in Fig. 14. Long period oscillations can be found for $I = 0.15\ \mu$M and $I = 0.42\ \mu$M or fast and slow recovery from inhibition and a range of inhibition rates. The

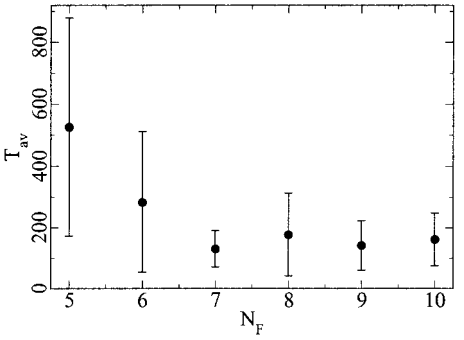

FIGURE 12 Average periods T_{av} for different numbers of additional clusters in focal sites.

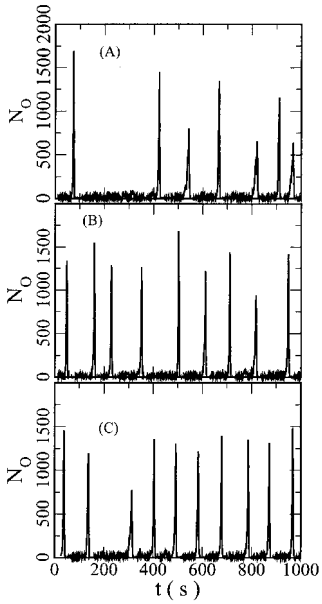

FIGURE 13 Simulations using different random realizations of cluster grids with identical average spatial characteristics. (*A*) $T_{av} = 177 \pm 135$ s, (*B*) $T_{av} = 112 \pm 24$ s, (*C*) $T_{av} = 103 \pm 29$ s. See Table 1 for further parameters.

nucleation characteristics are rather robust with respect to local dynamics. What is similar for the different simulations in Fig. 14 is the weak local coupling and the small average number of excitable channels per cluster of ≈5. Oscillation periods were sensitive to changes in these two parameters.

Especially, the sensitivity for the average number of excitable channels per cluster brings up the question for the deterministic limit. The deterministic limit assumes infinitely many channels per cluster while keeping the flux density and $\sqrt{N_K^{max}} R_s$ constant. The behavior of the system with increasing number of channels per cluster is shown in Fig. 15. While increasing N_K^{max} the single channel radius R_s was rescaled like $1/\sqrt{N_K^{max}}$ thus conserving the parameters entering the deterministic limit. Fig. 15 shows that T_{av} changes by a factor of 5 (if we ignore the first data point with very large period but very large standard deviation too) while going from 25–328 channels per cluster. A further increase of N_K^{max} strongly suggests that the deterministic limit is not oscillatory but is a stationary state with high activity compared to the activity between waves during long period oscillations (Fig. 16). That means that the oscillations are completely due to fluctuations i.e., stochastic channel behavior. Obviously, the fluctuations occurring with realistic channel numbers are large enough to leave the attractive region (stable manifold) of the high activity stationary state which is observed for channel numbers approaching the deterministic limit. I perturbed the system represented by the thick line in Fig. 16 *A* by increasing the number of open channels artificially by 500 (≈1% of the total channel number). A decrease of N_O to almost zero and a spike ensue the perturbation. That is very similar to the trajectory of the system with smaller N_K^{max} during an oscillation and suggests that oscillations can be imagined by assuming a very small residence time in the vicinity of the high activity stationary state.

I find again a high activity stationary state for larger IP_3 and large N_K^{max} (Fig. 17). That means that short period oscillations with small N_K^{max} too are due to fluctuations. However, there is a difference to the long period oscillations which can be perceived as nucleation phenomena. The short periods do not depend on the system size (data not shown)

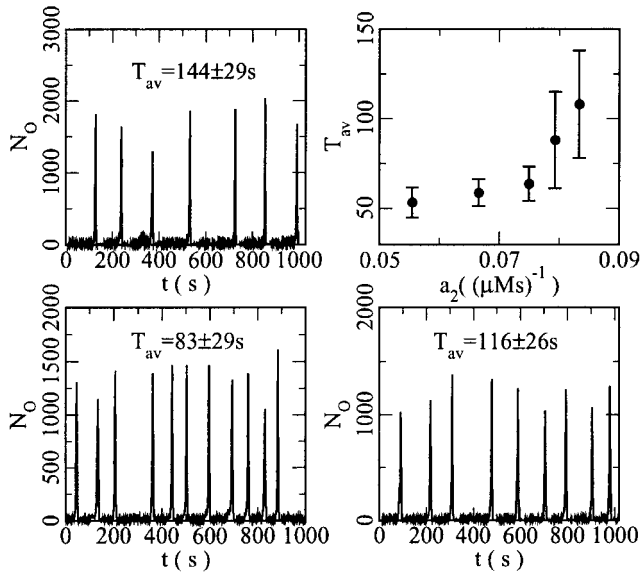

FIGURE 14 Simulations using a variety of parameter sets for the local dynamics. Parameters different from those in Table 1 are (*top left*) $B_{ex} = 60$ μM, $I = 0.18$ μM, $d_5 = 0.83\,s^{-1}$ (increased deactivation), (*top right*) T_{av} for different inhibition rate constants a_2 (note $a_2 = a_4$) $B_{ex} = 60$ μM, $I = 0.18$ μM, (*bottom left*) $B_{ex} = 60$ μM, $I = 0.42$ μM, $N_K^{max} = 13$, $d = 4.6$ μm, (*bottom right*) $B_{ex} = 60$ μM, $I = 0.15$ μM, $N_F = 7$.

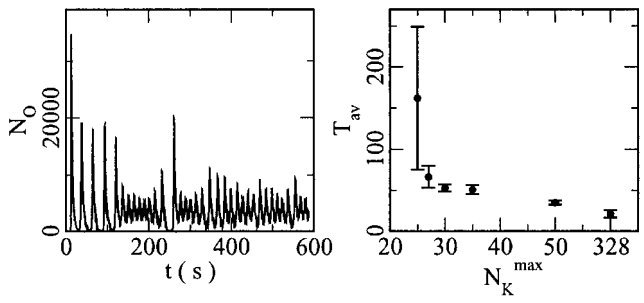

FIGURE 15 Simulations with different N_K^{max}. The single channel radius was chosen proportional to $1/\sqrt{N_K^{max}}$. (*Left*) Simulation with $N_K^{max} = 328$; (*right*) T_{av} dependent on $N_K^{max} \cdot B_{ex} = 60$ μM, $I = 0.15$ μM. See Table 1 for further parameters.

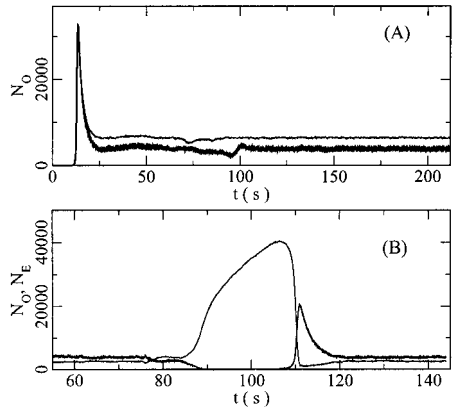

FIGURE 16 Simulations with $N_K^{max} = 1130$, $I = 0.15$ μM, and $N_F = 5$. The single channel radius was chosen proportional to $1/\sqrt{N_K^{max}}$ as explained in the text. (*A*) shows the case corresponding to Fig. 6 *A* (*thick line*) and with recovery from inhibition sped up by a factor of 2.5 (*thin line*). (*B*) shows N_O (*thick line*) and N_E (*thin line*). The simulation is that of panel *A* (*thick line*) but perturbed at $t = 75$ s. Despite the fact that I increased the number of open channels artificially with the perturbation the consequence is a decrease of N_O to almost zero followed by a spike and again stationary behavior.

and are in the range of the time scales of single channel dynamics.

Finally, I would like to present a comparison of simulation results with the data presented in (Marchant and Parker, 2001). Marchant et al. plot the periods and their standard deviation for a range of IP_3 concentrations. I compare these values with simulation data in Fig. 18 showing the relative standard deviation ($\Delta T_{av}/T_{av}$) versus T_{av}. The data in (Marchant and Parker, 2001) were obtained with 33 oocytes from five frogs. Accordingly, I included into the comparison

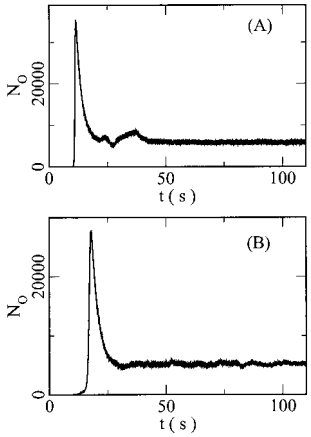

FIGURE 17 Simulations with $N_K^{max} = 546$, $I = 0.42$ μM in panel *A* and $N_K^{max} = 685$, $I = 0.27$ μM in panel *B*, both $N_F = 5$. The single channel radius was chosen proportional to $1/\sqrt{N_K^{max}}$ as explained in the text. (*A*) shows the case corresponding to Fig. 6 *C*. The system reaches a high activity stationary state for large times.

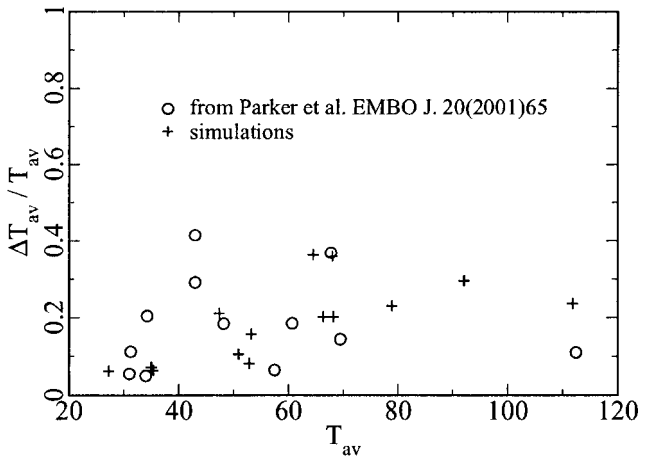

FIGURE 18 Comparison of the experimental data of Fig. 2 in Marchant and Parker (2001) with simulations. Shown is the relative standard deviation of $\Delta T_{av}/T_{av}$ versus T_{av}.

periods obtained with different parameters. The agreement especially in the range of 50- to 80-s periods is good. That confirms Parker's hypothesis that the stochastic part of periods is due to wave nucleation and that this process can be modeled with the simulation concept presented here.

DISCUSSION

I performed simulations inspired by the experiments by Parker and co-workers and Bootman and co-workers on initiation of global events by puffs. A first result is that I could model experimental findings by the approach explained in Materials and Methods. That approach allows for simulations in quite large spatial areas taking into account stochastic behavior of single channel subunits and the discrete array of channel clusters. That is possible because of an adiabatic approximation of the dynamics of Ca^{2+} and buffer concentrations and a superposition of single cluster profiles. The superposition will be a good approximation as long as the single cluster profiles of free Ca^{2+} are well localized on the length scale of typical cluster spacing. Most of the simulations I presented used a cluster spacing larger than 4 μm for which the superposition can be applied.

The adiabatic approximation implies that the concentration profile adapts immediately to the number of open channels. That means too that free Ca^{2+} goes to the base level concentration immediately upon closing of the last open channel within a vicinity of two to three cluster spacings. In other words, there is not any pacemaker Ca^{2+} if there are not any open channels around. However, the build up of pacemaker Ca^{2+} was found in experiments. To evaluate the importance of pacemaker Ca^{2+} in experiments when all channels in a wave nucleation area are closed I estimate the probability that this situation is given at an

arbitrary moment assuming an average puff duration of 300 ms. That probability is 7 10^{-5} for waves with periods between 15 and 50 s and ~0.2 for 60-s waves. The large difference between these two values arises from the large difference of puffs per time bin preceding a wave immediately given in (Marchant and Parker, 2001), Fig. 3 *C* and *E*. Hence, the typical situation is that there are clusters with open channels in the vicinity of closed clusters. In that situation, the Ca^{2+} coming from open channels is the larger contribution to the concentration value.

The adiabatic approximation may partially compensate for the lack of pacemaker Ca^{2+} with the rapid build up of the concentration profiles. Because of the immediate appearance of an increased concentration at clusters neighbored to one which just opened, the time these channels experience an increased concentration starts earlier compared to simulations with time dependent diffusion but will end earlier too.

Pacemaker Ca^{2+} will most likely increase the opening probability when there are not any open channels in the vicinity but the last open one has closed recently. One effect of a time-dependent simulation of the diffusion and hence a more realistic development of pacemaker Ca^{2+} could be a decrease of the variability of long periods because pacemaker Ca^{2+} would support the emergence of supercritical nuclei. However, if the nucleation probability is constant during the stochastic part of the period, it fixes the standard deviation as well. Therefore, the relative standard deviation could not depend on pacemaker Ca^{2+}. Pacemaker Ca^{2+} does not abolish variability of the period as the experimental data suggest. Moreover, pacemaker Ca^{2+} does not render the formation of supercritical nuclei a deterministic process as can be seen in Fig. 3 in (Bootman et al., 1997a). There, a global event does not nucleate even after pacemaker Ca^{2+} has been accumulated to a degree comparable to that one of supercritical nuclei. The role of pacemaker Ca^{2+} is the subject of ongoing simulations.

Ca^{2+} increases the opening probability per unit time p_o. For propagation, the probability that a cluster with open channels opens one channel of its neighbor clusters is relevant. As soon as one channel has opened, it dominates the Ca^{2+} concentration in its cluster. The increase of the opening probability caused by open channels at the neighboring cluster must be considerably larger than the probability of spontaneous opening to observe propagation. Local spontaneous events would dominate otherwise. If $c(r,t)$ denotes the concentration profile caused by a cluster with open channels at $r = 0$ and c_b the Ca^{2+} base level, $p_o(c_b)l = \int_l p_o(c(d,t))dt$ is required for propagation, with l being the average life time of puffs. Hence, if we observe propagation of release, the concentration profile of free Ca^{2+} caused by puffs reaches the neighboring clusters, i.e., it is meaningful to assume single cluster profiles. Moreover, propagation is the first global phenomenon observed while going from low to high IP_3. Therefore, single cluster profiles causing an essential increase of open probabilities at neighboring clusters exist for all regimes we have modeled.

The concentration of free Ca^{2+} at a distance d from a cluster with open channels $c(d,t)$ is of course affected by the adiabatic approximation. It monotonously increases up to a certain maximum upon opening of a cluster and then decreases again monotonously upon closing of the last open channel, if modeled with time dependent diffusion. I replace that smooth function by a stepwise function by the adiabatic approximation. The way to compare results of simulations using the adiabatic approximation with those using time dependent diffusion would be to compare the probability increase caused by a puff at its neighbor's site, i.e., the integrals $\int_l p_o(c(d,t))dt$ only. That is of course a weaker requirement than exact agreement of the time courses. The stationary single cluster profiles can be considered typical for puffs in the sense that they generate an increase in open probability comparable to that of puffs.

I could model a range of oscillation periods from 17 s to 2 min. The variability of the period increases with its average value but stays in the experimentally observed range. These findings are in good agreement with experimental results. Long periods are determined by the nucleation probability for a wave and not by a time scale of the single channel dynamics. Hence, processes prolonging inhibition or recovery from it are not necessary to achieve long periods in the case of nucleation oscillations. The parameters the nucleation process is most sensitive to are those influencing the life time of puffs, the number of channels per cluster which can be activated and spatial coupling, i.e., the average period depends on buffer concentration too. Lukyanenko et al. found in rat ventricular cardiac myocytes that wave frequency decreases with increasing EGTA concentration (Lukyanenko and Györke 1999). That supports my results for the wave nucleation regime.

The stochastic part of the period depends on the cell size as long as the number of focal sites increases with the cell size and therefore the probability that one focal site sets off a wave. The standard deviation of the average period decreases with increasing system size in the same way. The dependence on system size does not mean that nucleation oscillations occur in large cells only. It merely means that they occur at lower IP_3 in larger cells or in cells with more focal sites. However, the standard deviation at the same T_{av} is smaller in large systems with a few focal sites than in small systems with only one focal site.

Dupont et al. suggested another mechanism to prolong oscillation periods (Dupont and Swillens, 1995). That mechanism relies on fast removal of free Ca^{2+} from the channel mouth so that released Ca^{2+} cannot activate other channels of the same cluster. The nucleation mechanism I propose has less stringent requirements because it requires low IP_3 concentration and weak spatial coupling only. Another possibility to prolong Ca^{2+}-oscillation periods is a coupling to a phosphorylation–dephosphorylation cycle

like shown in (Gall et al., 2000) or receptor phosphorylation (LeBeau et al., 1999). However, most likely both is not the case in *Xenopus* oocytes and cannot account for the long period oscillations there.

The onset of oscillations by wave nucleation produces the right behavior of the amplitude with increasing IP_3. Oscillations start with large amplitudes and long periods and the amplitude and period decrease with increasing IP_3 (see Marchant and Parker, 2001). Short period oscillations occur at higher IP_3 concentration values. Note that the amplitude of puffs increases only slightly with the number of activatable channels. Hence, the decrease in period is mostly due to the increase of channel number and less to higher Ca^{2+} concentration. Short periods arise under conditions when many groups of clusters are able to set off a wave, not only focal sites. Hence, they depend less on coupling parameters and the system size. The finding that oscillations depend on the number of channels per cluster for high IP_3 rather than the number of focal sites implies that the results in that $[IP_3]$ range are valid for small cells too. Furthermore, the simulations indicate that the decrease of period with increasing IP_3 may be essentially due to increasing channel number rather than dependence of recovery rate on IP_3.

I found long period oscillations for single cluster profiles causing a 100- to 130-fold increase of binding probability for Ca^{2+} at the location of the cluster ($r = 0$) and approximately twofold at the neighboring cluster. That causes an increase in opening probability of the order 10^6 and 8 respectively, assuming that all subunits are in X_{00} and three of them need to bind Ca^{2+}. The value at $r = 0$ in terms of Ca^{2+} concentration seems rather low compared to simulations of release through a single channel with realistic current values. The computational effort necessary for the (long) simulations presented here does not allow for a comprehensive scan of the parameter space and hence I do not know, if these small values are a necessary condition for long periods to occur. In many simulations with higher concentrations long period oscillations were not observed. Short period oscillations or a high activity state could be found only. Our ongoing research addresses that question. If peak concentrations at the location of clusters as we used should turn out to be a necessary condition, it would mean that the binding probability needs to saturate at very high Ca^{2+} at values around 100 times base level or lower for nucleation oscillations to occur. Such a saturation was assumed in the model by Sneyd and Dufour (2002).

I found that periods depend on the very realization of a cluster field and not on its statistical characteristics only. That may be a simple explanation for different behavior of cells with otherwise similar characteristics. It suggests too that there are optimal configurations for a certain period T_{av} and $\Delta T_{av}/T_{av}$ analogously to the finding by Shuai et al. of optimal channel numbers per cluster for quasi periodic behavior of a single cluster (Shuai and Jung, 2002). I have not performed a special search for such an optimal N_K^{max} here because I used variable numbers of channels per cluster within a single cluster field.

The finding that the deterministic limit of systems with low and high concentration of IP_3 is a high activity stationary state is the most important result with respect to modeling concepts. That means that for some cells deterministic differential equations do not capture the right mechanism of oscillations. The oscillations in systems with small numbers of channels per cluster which can be activated by the binding of Ca^{2+} can be due to fluctuations. They may be caused by wave nucleation, fluctuations across a threshold or escape from a stationary state of a bistable system. I showed the first mechanism to be responsible for the long period oscillations of the current system.

I do not know yet the way the channel population uses to avoid the high activity stationary state at small channel numbers per cluster. Obviously, that state has a small basin of attraction. If one assumes that the dynamics can be reduced to a plane in phase space, as many deterministic models do (Tang and Othmer, 1996), a phase space structure like shown in Fig. 19 seems plausible. It shows a bistable system with the ingoing separatices of the saddle passing close by the stationary states. The separatrix close to the lower stationary state provides the excitability of the low activity stationary state. The upper stationary state is a focus. The trajectory of the system during a wave in the long period regime is shown in Fig. 19 *A*. Nucleation corresponds to crossing the separatrix close to the lower stationary state because of fluctuations. That is followed by motion roughly along a deterministic trajectory leading into the vicinity of the upper stationary state. The second ingoing separatrix is very close to that state at low IP_3. Hence, fluctuations push the system across it whenever it approaches the high activity stationary state. Finally, it relaxes to the lower stationary state again in a deterministic-like way.

The distance between the separatrix and the upper stationary state increases with increasing IP_3. Therefore, fluctuations do not push the system across it when approaching the stationary state under these conditions. The short period oscillations could now be comprehended as

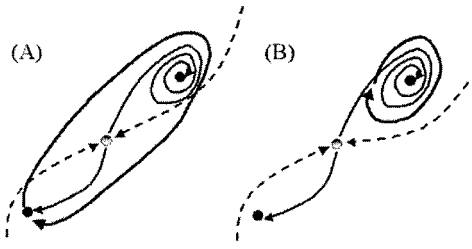

FIGURE 19 Phase space structure which could be imagined as underlying the observed behavior of the stochastic system. Stable stationary point (*filled dots*); saddle point (*shaded dots*); outgoing separatrices (*thin solid lines*) ingoing separatrices (*dashed lines*); trajectories (*thick solid lines*) (*A*) low $[IP_3]$, (*B*) high $[IP_3]$.

a fluctuation driven transition to an outer revolution of the spiral-like separatrix when the system approaches the stationary state followed again by a relaxation toward the stationary state similar to the deterministic dynamics. That picture would imply that the single channel dynamics is crucial for setting the short periods. The overall mechanism suggested here is similar to that one described in Garcia-Ojalvo and Schimansky-Geier (2000) for a bistable stochastic FitzHugh-Nagumo model. There, the stochastic process setting the period is escape from stationary states too. However, the short period mechanism described here is not observed in that model.

The stationary high activity state reflects the behavior of the DeYoung-Keizer model. Such a state can be reached in the deterministic model by increasing the Ca^{2+} flux through channels which causes an increase of the cytosolic Ca^{2+} concentration. That situation occurs at the location of open channels in a discrete model. The high local Ca^{2+} concentration suppresses oscillatory behavior which needs intermediate Ca^{2+} concentrations. My findings in simulations approaching the deterministic limit suggest that the oscillatory regime in models is lost during the transition from spatially continuous channel density to spatial discreteness of the channel clusters while keeping the average flux density constant. Fluctuations compensate for that by restoring the ability for oscillatory behavior.

A high activity stationary state as one stable state of a bistable dynamics was found in a model for *Xenopus* oocytes with energized mitochondria too (Falcke et al., 1999; Falcke et al., 2000a). That state was stabilized by the interaction of the Ca^{2+} handling of mitochondria and the ER. The occurrence of such a state in different models of intracellular Ca^{2+} dynamics supports the idea that the cytosol might be a bistable system for high IP_3. That stationary state of the local dynamics led to the disappearance of spiral waves without abolishing less curved waves in the model with energized mitochondria because of a gap in the dispersion relation (Falcke et al., 2000a). Experimentally as well as in the model, it was found that the cytosol might stay for a rather long time in a high activity stationary state and then leave it by a front of low Ca^{2+} release or as we now know because of fluctuations (Figs. 16 *B* and 11 *A*) and Fig. 3, *E* and *F* in Falcke et al. (1999). Bistability was assumed as well in a model for the fertilization wave in *Xenopus* oocyte (Wagner et al., 1998).

The interplay between puffs and waves described in the introduction for experiments and as a result of the simulations is not unique to *Xenopus* oocytes. Puffs are observed e.g., in HeLa cells as well (Bootman et al., 1997b). HeLa cells are much smaller than *Xenopus* oocytes (Bootman et al., 1997b). Puff sites show a spacing of 2–7 μm (Thomas et al., 1998). Hence, there are less puff sites than in *Xenopus* oocytes and stochastic effects could be even more important. Moreover, global release events are initiated by cooperative activity of several puff sites too. That demonstrates the existence of a parameter range with weak spatial coupling. Hence, I expect that the results of this report concerning the role of fluctuations are important for HeLa cells and other small cells too. However, small cells require a careful consideration of the dynamics of base level concentrations. Another reason that I focused on *Xenopus* oocytes is that because of the size of the cell wave phenomena can be observed and the link between oscillations and pattern formation can be established.

Partial differential equations for the concentration fields of Ca^{2+} and buffers

The complete system of PDEs for all concentration variables reads:

$$\begin{aligned}
\frac{\partial c}{\partial t} &= D\nabla^2 c + (P_\mathrm{l} + P_\mathrm{c})(E - c) - P_\mathrm{p}\frac{c^2}{K_\mathrm{d}^2 + c^2} \\
&\quad - k_\mathrm{s}^+ (B_\mathrm{s} - b_\mathrm{s})c + k_\mathrm{s}^- b_\mathrm{s} \\
&\quad - k_\mathrm{m}^+ (B_\mathrm{m} - b_\mathrm{m})c + k_\mathrm{m}^- b_\mathrm{m} \\
&\quad - k_\mathrm{ex}^+ (B_\mathrm{ex} - b_\mathrm{ex})c + k_\mathrm{ex}^- b_\mathrm{ex} \\
\frac{\partial E}{\partial t} &= D_\mathrm{E}\nabla^2 E - \gamma\left[(P_\mathrm{l} + P_\mathrm{c})(E - c) - P_\mathrm{p}\frac{c^2}{K_\mathrm{d}^2 + c^2}\right] \\
&\quad - k_\mathrm{Es}^+ (B_\mathrm{Es} - b_\mathrm{Es})E + k_\mathrm{Es}^- b_\mathrm{Es} \\
&\quad - k_\mathrm{Em}^+ (B_\mathrm{Em} - b_\mathrm{Em})E + k_\mathrm{Em}^- b_\mathrm{Em} \\
\frac{\partial b_\mathrm{s}}{\partial t} &= k_\mathrm{s}^+ (B_\mathrm{s} - b_\mathrm{s})c - k_\mathrm{s}^- b_\mathrm{s} \\
\frac{\partial b_\mathrm{m}}{\partial t} &= D_\mathrm{m}\nabla^2 b_\mathrm{m} + k_\mathrm{m}^+ (B_\mathrm{m} - b_\mathrm{m})c - k_\mathrm{m}^- b_\mathrm{m} \\
\frac{\partial b_\mathrm{ex}}{\partial t} &= D_\mathrm{ex}\nabla^2 b_\mathrm{ex} + k_\mathrm{ex}^+ (B_\mathrm{ex} - b_\mathrm{ex})c - k_\mathrm{ex}^- b_\mathrm{ex} \\
\frac{\partial b_\mathrm{Es}}{\partial t} &= k_\mathrm{Es}^+ (B_\mathrm{Es} - b_\mathrm{Es})E - k_\mathrm{Es}^- b_\mathrm{Es} \\
\frac{\partial b_\mathrm{Em}}{\partial t} &= D_\mathrm{Em}\nabla^2 b_\mathrm{Em} + k_\mathrm{Em}^+ (B_\mathrm{Em} - b_\mathrm{Em})E - k_\mathrm{Em}^- b_\mathrm{Em}. \qquad (3)
\end{aligned}$$

Here I define

$$A = Dc + D_\mathrm{ex} b_\mathrm{ex} + D_\mathrm{m} b_\mathrm{m} + \frac{1}{\gamma}(D_\mathrm{E} E + D_\mathrm{Em} b_\mathrm{Em}) \qquad (4)$$

and the total Ca^{2+} concentration C_T:

$$C_\mathrm{T} = c + b_\mathrm{s} + b_\mathrm{m} + b_\mathrm{ex} + \frac{1}{\gamma}(E + b_\mathrm{Es} + b_\mathrm{Em}) \qquad (5)$$

$$\begin{aligned}
\frac{\partial C_\mathrm{T}}{\partial t} &= \nabla^2\left(Dc + D_\mathrm{ex} b_\mathrm{ex} + D_\mathrm{m} b_\mathrm{m} + \frac{1}{\gamma}(D_\mathrm{E} E + D_\mathrm{Em} b_\mathrm{Em})\right) \\
\frac{\partial C_\mathrm{T}}{\partial t} &= \nabla^2 A. \qquad (6)
\end{aligned}$$

Solving for the stationary solution of C_T^0 uncouples that PDE from the others and leads to:

$$\nabla^2 A = 0.$$

The general solution of that equation in two spatial dimensions is $constant_1 + constant_2 \ln r$ (with r being the space coordinate). Because $\ln r$ does not match the boundary conditions (zero flux or periodic) we reach $A = A^0 = constant$. We use A^0 to replace E^0

$$E^0 = \frac{\gamma}{D_E}\left(A^0 - Dc^0 - D_{ex}b^0_{ex} - D_m b^0_m - \frac{D_{Em}b^0_{Em}}{\gamma}\right) \quad (7)$$

and solve for the stationary solution of the concentrations obeying:

$$\begin{aligned}
0 &= D_m\nabla^2 b^0_m + D_{ex}\nabla^2 b^0_{ex} + D\nabla^2 c^0 + (P_l + P_c)(E^0 - c^0) \\
&\quad - P_p\frac{(c^0)^2}{K_d^2 + (c^0)^2} \\
0 &= D_m\nabla^2 b^0_m + k^+_m(B_m - b^0_m)c^0 - k^-_m b^0_m \\
0 &= D_{ex}\nabla^2 b^0_{ex} + k^+_{ex}(B_{ex} - b^0_{ex})c^0 - k^-_{ex}b^0_{ex} \\
0 &= D_{Em}\nabla^2 b^0_{Em} + k^+_{Em}(B_{Em} - b^0_{Em})E^0 - k^-_{Em}b^0_{Em} \\
b^0_s &= \frac{B_s c^0}{K_s + c^0} \\
b^0_{Es} &= \frac{B_{Es}E^0}{K_{Es} + E^0}. \qquad (8)
\end{aligned}$$

A^0 is determined by

$$\frac{1}{V}\int_V dV C_T(A^0, r) = \frac{1}{V}\int_V dV c^0(A^0, r) + b^0_s(A^0, r) + b^0_m(A^0, r) + b^0_{ex}(A^0, r) + \frac{1}{\gamma}(E^0(A^0, r) + b^0_{Es}(A^0, r) + b^0_{Em}(A^0, r)) = C_0. \quad (9)$$

The solution of that integral equation depends on the configuration of open channels $\mathbf{N_O}(t)$. That can be understood by imagining the extreme case of redistributing a large fraction of free Ca^{2+} to immobile buffers by release. The release would decrease the value of A^0 because immobile buffers do not contribute to it.

The system of Eqs. 8 and 9 was solved every time $\mathbf{N_O}(t)$ changed for the simulations shown in Figs. 2 and 3. I used the single cluster profile approach for fast localized variables in all other simulations. The single cluster solutions were determined by solving Eq. 8 with a single cluster site centered at $r = 0$. The value of A^0 was determined by Eq. 9 for the concentration fields on the whole area.

I solved all partial differential equations by a multigrid method according to Press et al. (1992). I used a spatial discretization of 4 nm to calculate single cluster profiles. The time step size in stochastic simulations was chosen so that the probability for a transition in a cluster was ~1% and hence for all clusters within an interaction radius ~7%. Because only about one quarter of the transitions changes the open state of channels that yields ~2% probability per time step for a transition changing rates of other transitions within the interaction radius. Test runs with one half of that time step and one quarter confirmed the choice. I used random number generators taken from Press et al. (1992).

REFERENCES

Berridge, M., M. Bootman, and P. Lipp. 1998. Calcium - a life and death signal. *Nature*. 395:645–648.

Bootman, M., M. Berridge, and P. Lipp. 1997a. Cooking with calcium: The recipes for composing global signals from elementary events. *Cell*. 91:367–373.

Bootman, M., E. Niggli, M. Berridge, and P. Lipp. 1997b. Imaging the hierarchical Ca^{2+} signaling in HeLa cells. *J. Physiol.* 499:307–314.

Callamaras, N., and I. Parker. 2000. Phasic characteristics of elementary Ca^{2+} release sites underlies quantal responses to IP_3. *EMBO J.* 19:3608–3617.

Callamaras, N., J. Marchant, X.-P. Sun, and I. Parker. 1998. Activation and coordination of $insp_3$-mediated elementary Ca^{2+} events during global Ca^{2+} signals in Xenopus oocytes. *J. Physiol. (Lond.)*. 509:81–91.

DeYoung, G., and J. Keizer. 1992. A single-pool inositol 1,4, 5-trisphosphate-receptor-based model for agonist-stimulated oscillations in Ca^{2+} concentration. *Proc. Natl. Acad. Sci. USA*. 89: 9895–9899.

Dupont, G., and S. Swillens. 1995. Quantal release, incremental detection, and long-period Ca^{2+} oscillations in a model based on regulatory Ca^{2+}-binding sites along the permeation pathway. *Biophys. J.* 71: 1714–1722.

Falcke, M. 2003. Buffers and oscillations in intracellular Ca^{2+} dynamics. *Biophys. J.* 84:28–41.

Falcke, M., J. Hudson, P. Camacho, and J. Lechleiter. 1999. Impact of mitochondrial Ca^{2+} cycling on pattern formation and stability. *Biophys. J.* 77:37–44.

Falcke, M., M. Or-Guil, and M. Bär. 2000a. Dispersion gap and localized spiral waves in a model for intracellular Ca^{2+} dynamics. *Phys. Rev. Lett.* 84:4753–4756.

Falcke, M., L. Tsimring, and H. Levine. 2000b. Stochastic spreading of intracellular Ca^{2+} release. *Phys. Rev.E.* 62:2636–2643.

Gall, D., E. Baus, and G. Dupont. 2000. Activation of the liver glycogen phosphorylase by Ca^{2+} oscillations: a theoretical study. *J. Theor. Biol.* 207:445–454.

Garća-Ojalvo, J., and L. Schimansky-Geier. 2000. Excitable structures in stochastic bistable media. *J. Stat. Phys.* 101:473–481.

Hempel, H., L. Schimansky-Geier, and J. García-Ojalvo. 1999. Noise-sustained pulsating patterns and global oscillations in subexcitable media. *Phys. Rev. Lett.* 82:3713–3716.

Ilyin, V., and I. Parker. 1994. Role of cytosolic Ca^{2+} in inhibition of $InsP_3$-evoked Ca^{2+} release in Xenopus oocytes. *J. Physiol.* 477:503–509.

Jung, P., and P. Galley. 2000. The heartbeat of extended clocks. *Ann. Phys.* 9:697–704.

Keizer, J., and G. DeYoung. 1994. Simplification of a realistic model of IP_3-induced Ca^{2+} oscillations. *J. Theor. Biol.* 166:431–442.

LeBeau, A., D. Yule, G. Groblewski, and J. Sneyd. 1999. Agonist-dependent phosphorylation of the inositol 1,4,5-trisphosphate receptor - a possible mechanism for agonist-specific calcium oscillations in pancreatic acinar cells. *J. Gen. Physiol.* 113:851–871.

Lechleiter, J., S. Girard, E. Peralta, and D. Clapham. 1991. Spiral calcium wave propagation and annihilation in Xenopus laevis oocytes. *Science*. 252:123–126.

Lukyanenko, V., and S. Györke. 1999. Ca^{2+} sparks and Ca^{2+} waves in saponin-permeabilized rat ventricular myocytes. *J. Physiol.* 521:575–585.

Mak, D., and J. Foskett. 1998. Effects of divalent cations on single-channel conduction properties of Xenopus IP_3 receptor. *Am. J. Physiol.* 275:C179–C188.

Mak, D., S. McBride, and J. Foskett. 2001. Regulation by Ca^{2+} and Inositol 1,4,5-trisphosphate ($InsP_3$ of single recombinant type 3 $InsP_3$ receptor channels: Activation uniquely distinguishes type 1 and type 3 $InsP_3$ receptors. *J. Gen. Physiol.* 117:435–446.

Mak, D., S. McBride, V. Raghuram, Y. Yue, S. Joseph, and J. Foskett. 2000. Single-channel properties in endoplasmic reticulum membrane of recombinant type 3 inositol trisphosphate receptor. *J. Gen. Physiol.* 115:241–255.

Marchant, J., and I. Parker. 2001. Role of elementary Ca^{2+} puffs in generating repetitive Ca^{2+} oscillations. *EMBO J.* 20:65–76.

Marchant, J., N. Callamaras, and I. Parker. 1999. Initiation of IP_3-mediated Ca^{2+} waves in Xenopus oocytes. *EMBO J.* 18:5285–5299.

Moraru, I., E. Kaftan, B. Ehrlich, and J. Watras. 1999. Regulation of type 1 Inositol 1,4,5-trisphosphate-gated calcium channels by $InsP_3$ and calcium. *J. Gen. Physiol.* 113:837–849.

Ölveczky, B., and A. Verkman. 1998. Monte carlo analysis of obstructed diffusion in three dimensions: application to molecular diffusion in organelles. *Biophys. J.* 74:2722–2730.

Patel, S., S. Joseph, and A. Thomas. 1999. Molecular properties of inositol 1,4,5-trisphosphate receptors. *Cell Calcium.* 25:247–264.

Press, W., S. Teukolsky, W. Vetterling, and B. Flannery. 1992. Numerical recipes in C. 2nd ed, Cambridge University Press, Cambridge.

Shuai, J., and P. Jung. 2002. Optimal intracellular calcium signaling. *Phys. Rev. Lett.* 88:U252–U255.

Sneyd, J., and J.-F. Dufour. 2002. A dynamic model of the type-2 inositol trisphosphate receptor. *Proc. Natl. Acad. Sci. USA.* 99:2398–2403.

Sneyd, J., J. Keizer, and M. Sanderson. 1995. Mechanisms of calcium oscillations and waves: a quantitative analysis. *FASEB J.* 9:1463–1472.

Sun, X.-P., N. Callamaras, J. Marchant, and I. Parker. 1998. A continuum of $insp_3$-mediated elementary Ca^{2+} signaling events in Xenopus oocytes. *J. Physiol. (Lond.).* 509:67–80.

Swillens, S., P. Champeil, L. Combettes, and G. Dupont. 1998. Stochastic simulation of a single inositol 1,4,5-trisphoasphate-sensitive Ca^{2+} channel reveals repetitive openings during blip-like Ca^{2+} transients. *Cell Calcium.* 23:291–302.

Tang, Y., and H. Othmer. 1996. Simplification and analysis of models of calcium dynamics based on IP_3-sensitive calcium channel kinetics. *Biophys. J.* 70:246–263.

Taylor, C. 1998. Inositol trisphosphate receptors: Ca^{2+}-modulatd intracellular Ca^{2+} channels. *Biochim. Biophys. Acta.* 1436:19–33.

Thomas, D., P. Lipp, M. Berridge, and M. Bootman. 1998. Hormone-stimulated elementary Ca^{2+} signals are not stereotypic, but reflect activation of different size channel clusters and variable recruitment of channels within a cluster. *J. Biol. Chem.* 273:27130–27136.

Thomas, D., P. Lipp, S. Tovey, M. Berridge, W. Li, R. Tsien, and M. Bootman. 1999. Microscopic properties of elementary Ca^{2+} release sites in non-excitable cells. *Curr. Biol.* 10:8–15.

Tsien, R., and R. Tsien. 1990. Calcium channels stores and oscillations. *Annu. Rev. Cell Biol.* 6:715–760.

Wagner, J., Y.-X. Li, J. Pearson, and J. Keizer. 1998. Simulation of the fertilization Ca^{2+} wave in Xenopus laevis eggs. *Biophys. J.* 75:2088–2097.